Influence of the Submerged Arc Welding in the Mechanical Behaviour of the P355NL1 Steel. Part I: Analysis of the Cyclic Elastoplastic Behaviour

Abílio M.P. De Jesus
University of Trás-os-Montes and Alto Douro, Engineering Department, Quinta de Prados, 5000-911 Vila Real, Portugal
ajesus@utad.pt

Alfredo S. Ribeiro
University of Trás-os-Montes and Alto Douro, Engineering Department, Quinta de Prados, 5000-911 Vila Real, Portugal

António A. Fernandes
University of Porto – Faculty of Engineering, Rua Dr. Roberto Frias, 4200-465 Porto, Portugal

Abstract. *A normalised fine grain carbon low alloy steel, P355NL1 (EN10028-3), intended for service in welded pressure vessels has been investigated. Applications with this steel usually require intensive use of welds. A very common welding process that is used in the manufacturing of pressure vessels is the submerged arc welding. This welding process is often automated in order to perform the main seam welds making the body of the vessels. The influence of the automated submerged arc welding in the mechanical properties is investigated. In this paper, the cyclic elastoplastic behaviour of the base material (P355NL1 steel) is compared with the corresponding behaviour of the welded material. Several series of small and smooth specimens made of base and welded materials were cyclic tested. The cyclic elastoplastic behaviours of the materials are described, using relations available in the literature, and compared. The shape of hysteresis loops are conveniently modelled, taking into account the observed non-Masing behaviour of the base and welded materials. Some important cyclic elastoplastic phenomena are also illustrated.*

Keywords*: P355NL1 steel, submerged arc welding, cyclic behaviour, elastoplasticity*

1. Introduction

Pressure vessels are often subjected to cyclically varying stresses or strains due to pressure fluctuations and/or external loads variations, which can induce fatigue damage at the highly stressed or strained locations leading, frequently, to premature failures in equipment intended for long life applications, as reported in many investigations (Taylor *et al*, 2001). The European Pressure Equipment Directive, PD 97/23/EC (EC, 2001) in its Annex I, emphasizes the need for taking into account all foreseeable degradation mechanisms commensurate with the intended use of the equipment, including fatigue. The recommended procedures for fatigue analysis are those included in design codes of practice such as the ASME VIII – Div. 2 (ASME, 2001), the PD5500 (BSI, 2003) and the EN 13445 standard (CEN, 2002). However, code based procedures are often unable to deal with some complex problems (e.g. complex geometry and/or loading). They usually give an overall prediction which does not allow the fully understanding of the influence of the relevant parameters contributing for the fatigue damage. Thus, alternative procedures that have been proposed can be used in order to complement the code based rules. The most important alternative assessment methods are the local approaches (Radaj and Sonsino, 1998).

The success of the application of the local approaches to fatigue is dependent on the availability of specific experimental data about the materials to be analyzed, which usually constitutes a difficulty to the implementation of such approaches. This problem can be even more critical if the studied location is a welded zone, which can be considered a compound of several distinct materials: base metal, weld metal and heat affected zone. Weldments in steel structures are heterogeneous both in microstructure and mechanical properties. It is noted that the cyclic stress/strain behaviour, fatigue damage mechanism, fatigue crack initiation and growth rate are different in these three welded zones.

The authors have investigated intensively the steel plate P355NL1 (EN10028-3) (CEN, 2003), with 5.1 mm thickness, which is a weldable fine grain carbon low alloy steel, delivered in the normalized condition and intended for pressure service purposes where notch toughness is of high importance. Despite the intensive use of this steel in fabrication of modern pressure vessels or pressure equipment, very limited and non-systematic data exists on its fatigue behaviour. In a recent publication (De Jesus *et al*, 2005), the authors described the cyclic elastoplastic and the low and high cycle fatigue behaviours of the P355NL1 steel. Now, in this paper, authors make a comparison of the mechanical behaviour between the P355NL1 steel and the welded material, resulting from the submerged arc welding process, which is a very important welding process in the manufacturing of pressure vessels. This paper first describes the investigated materials; after, the complete experimental program is depicted. Finally, the comparison of the cyclic elastoplastic behaviours between the materials is carried out. The cyclic stress-strain curves, the shape of the hysteresis loops and typical cyclic behaviours, such as the cyclic softening/hardening (Lemaitre and Chaboche, 1990), cyclic creep (Chaboche, 1994) or mean stress relaxation (Dowling, 1998), are used in the comparison. The research documented in this paper is of extreme importance if a local approach to fatigue plus Linear Elastic Fracture Mechanics have to be applied to assess the main welds of pressure vessels. Similar works can be found in literature, based on different materials (Higashida *et al* (1978), Lawrence *et al* (1978), Cheng *et al*, 1996).

2. Fatigue assessment based on local approaches

The local approaches can be used as important alternatives to the code based procedures for fatigue assessment of structural details, including pressure vessel or pressure vessel type details. They can also be applied to complement or refine global predictions resulting from the application of code based procedures. Very common local approaches are based on the application of strain-life relations and are usually used to predict only the initiation of macroscopic cracks (Truchon (1982) and Costa and Ferreira, (1993)). These approaches are often applied in conjunction with the Linear Elastic Fracture Mechanics in order to predict the total failure of components, including both initiation and propagation of macroscopic cracks (Ribeiro (1993), Jakubczak *et al* (1996), Ribeiro *et al* (2001), De Jesus (2004)).

The success of a prediction based on the application of strain-life relations depends on the correct knowledge of the corresponding strain-life relation of the material, at the critical location. Also, the correct estimation of the strain history experienced by the material, at same critical location, is required to achieve good results. The strain history estimation should be carried out using the cyclic elastoplastic relations of the material at the location of interest.

Welds are typical critical details of pressure vessels (Curney, 1979). Fatigue cracks usually initiate at weld toes or weld roots which generally correspond to base material affected by the heat introduced by the welding process or to the welded material, as illustrated in Fig. 1. Thus, the assessment of welded joints, using local approaches, should take into account the correct properties of these materials. Due to difficulties in obtaining the required properties of the heat affected zone (HAZ) and welded material (WM), some authors (Cruz *et al*, 2000) have adopted the properties of the base material (BM) in the analysis of the welded joints, regardless the failure location.

The properties of the HAZ and WM can be determined indirectly by means of hardness measurements (Testin *et al*, 1987), or directly by testing specimens containing the referred materials in its gauge length (Cheng *et al*, 1996). In many cases, it is impossible to extract specimens, from welded details, containing the desired material in the gauge length. For these situations, some authors try to reproduce the desired materials applying adequate heat treatments to the gauge length of the specimens (Higashida *et al*, 1978).

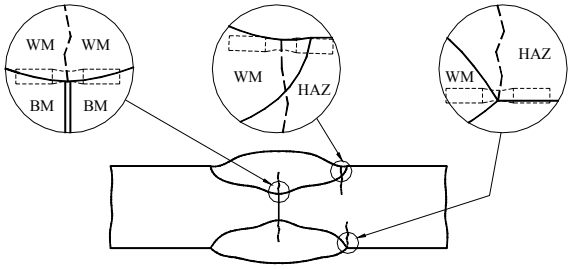

Figure 1. Typical crack initiation locations for a welded joint.

The authors propose, in this paper, the evaluation of the cyclic elastoplastic properties of the welded material and a comparison with the properties of the base material, which were already reported in a recent paper (De Jesus *et al*, 2005). The cyclic elastoplastic properties of the welded material were evaluated using specimens extracted from a welded detail in such a way that specimens have welded material in their gauge length. All properties are compared with the properties of the base material, the P355NL1 steel.

3. Materials characterization

In this paper, a comparison of the cyclic elastoplastic behaviour between a base and welded materials is performed. The base material is the carbon low alloy steel P355NL1, delivered in the form of plates with 5.1 mm thickness. This designation is according to the EN10028-3 standard (CEN, 2003). This steel has the former designation of TStE355, specified in the DIN 17102 standard (DIN, 1983). This steel is a weldable normalized fine grain structural steel, applied for pressure vessel purposes with special requirements for low temperatures. The chemical composition and basic mechanical properties are presented in Tab. 1 and Tab. 2, respectively. The welded material was produced using the automated submerged arc welding. Table 3 summarizes the main characteristics of the welding process, including the designations and chemical compositions of the flux and filler material and the welding parameters.

Table 1. Chemical composition of the P355NL1 steel (% weight).

C	Si	Mn	P	S	Al	Mo	Nb	Ni	Ti	V	Cu	Cr
0.144	0.199	1.443	0.018	0.006	0.034	0.001	0.009	0.037	0.001	0.003	0.059	0.031

Table 2. Monotonic strength and elastic properties of the P355NL1 steel (mean and standard deviations) (De Jesus *et al*, 2005).

Tensile strength, σ_{UTS} (MPa)	568 ± 3.4	Elongation, ε_r (%)	30 ± 2.6
Yield strength, $\sigma_{0.1\%}$ (MPa)	390 ± 12.1	Young modulus, E (GPa)	205.2 ± 2.0
Yield strength, $\sigma_{0.2\%}$ (MPa)	418 ± 6.2	Poisson coefficient, ν	0.275

Table 3. Main characteristics of the automated submerged arc welding process.

Designation/ General Characteristics		**Brand/reference**			**Classification AWS A5.17**			**Diameter**
	Filler Material	L60			EL12			3.2 mm
	Flux	780			F7 A0 - EL12			-
Chemical Composition (% weight)	**Filler material**	*C*	*Si*	*Mn*	*P*	*S*	*Cr*	*Ni*
		0.09	0.04	0.45	<0.01	<0.01	0.017	0.026
		Mo	*Cu**	*V*	*Al*	* Before the covering with *Cu*		
		0.01	0.015	<0.01	<0.01			
	Flux	*Mo*	*Zr*	*Mg*	*Ni*	*Fe*	*Mn*	*Cr*
		0.13	0.14	1.03	0.01	4.17	11.52	0.11
		V	*Ti*	*Ca*	*Si*	*K*	*Al*	
		0.14	5.28	5.8	6.77	0.47	19.12	

Welding Parameters	**Welding position (EN 288-3:1992)**	**Intensity (Amp.)**		**Tension (Volt)**	**Velocity (mm/min)**	
		Pass 1	*Pass 2*		*Pass 1*	*Pass 2*
	PA	450	500	32	700	650

Figure 2 illustrates the three typical microstructures observed in a weld, namely the structures of the base material, welded material and the material affected by the heat generated by the welding process. The base material presents a typical ferrite-perlite grained-refined microstructure. The plate rolling direction is well defined in the microstructure. The heat introduced by the welding process produces a refinement of the perlite zones and partially destroys the preferential grain orientation introduced by the lamination process. The microstructure of the welded material corresponds to a gross microstructure resulting from the cooling process.

Figure 3 summarizes the results of a hardness testing preformed on the welded joint. The hardness test was conducted according to the ISO 6507 and EN 288-3 standards. The calculated hardness corresponds to the Vickers hardness, measured with a 98 N testing load. The base, heat affected and welded materials presented a mean Vickers hardness of 149, 158 and 172, respectively.

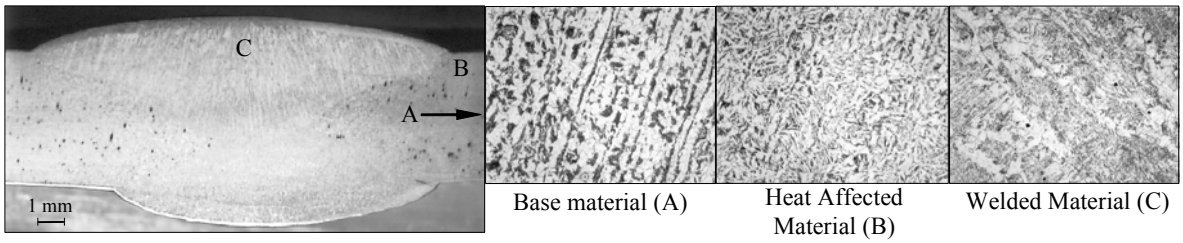

Figure 2. Microstructures resulting from the automated submerged arc welding (magnification 500×).

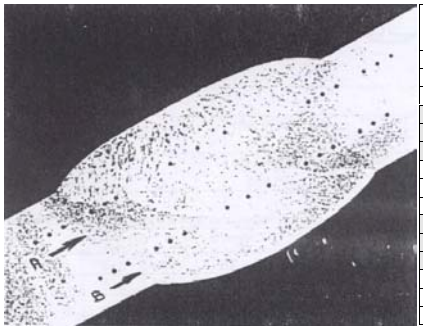

Nº	Location A		Location B	
	HV10	Zone	HV10	Zone
1	156	BM	149	BM
2	154	BM	149	BM
3	151	BM	146	BM
4	156	HAZ	141	HAZ
5	170	HAZ	154	HAZ
6	178	HAZ	156	HAZ
7	181	WM	160	WM
8	170	WM	170	WM
9	173	WM	176	WM
10	160	HAZ	154	HAZ
11	158	HAZ	156	HAZ
12	151	HAZ	156	HAZ
13	147	BM	149	BM
14	143	BM	147	BM
15	143	BM	149	BM

Figure 3. Hardness measurements on the butt welded joint.

4. Experimental details

The experimental work included tests of small and smooth specimens. The geometry and dimensions of those specimens are illustrated in Fig. 4 and are in agreement with the ASTM E606 standard (ASTM, 1998). Nine series of specimens were tested, four under strain control ($2\times R_\varepsilon=-1$, $2\times R_\varepsilon=0$) and five under stress control ($2\times R_\sigma=-1$, $R_\sigma=-0.5$, $2\times R_\sigma=0$), resulting a total of 127 tested specimens, as indicated in Tab. 4. Five series of specimens are made of base material; four series have welded material at the gauge length. The specimens with welded material at the gauge length were cut from two plates of base material that were butt welded before the cutting process. After, the welds of the specimens were flush grounded. No stress relief treatment was applied.

The specimens were cyclic tested under a tensile/compressive uniaxial stress state, until failure. All experiments were carried out on a close-loop servohydraulic machine (model INSTRON® 8801), rated to 100 kN. A sinusoidal waveform was used as command signal. All series were tested under constant strain or stress amplitudes. All tests were carried out at room-temperature in air. The longitudinal strain was measured using a longitudinal extensometer (model INSTRON® 2620-602) with a base length equal to 12.5 mm and limit displacements of ±2.5 mm. Cyclic tests carried out in low cycle fatigue regime ($N_f<5\times10^4$ cycles) had their frequency adjusted to result an average strain rate of 0.008/s. For high cycle fatigue regimes ($N_f>5\times10^4$ cycles) the maximum frequency considered was 20Hz.

5. Results and discussion

5.1. Typical cyclic behaviours

Some of the most important typical cyclic behaviours of the base material – the P355NL1 steel – were already identified in a recent paper (De Jesus, 2005). In this paper, a comparison of the cyclic behaviours between the base and welded materials is established. The cyclic tests carried out under strain control (series 2A and 2B) indicated that the base material exhibits cyclic softening or cyclic hardening depending on the strain amplitude. For larger strain amplitudes the material suffers a quick hardening followed by stabilization. For small strain amplitudes the material suffers a continuous softening. The graph of Fig. 5a, obtained with tests conducted under controlled fully-reversed strain (series 2A), illustrates this behaviour for the base material. De Jesus *et al* (2005) also illustrates the softening/hardening behaviour of the base material for tests conducted under controlled tensile-mean-strain with null strain ratio (series 2B) and it was concluded that the material essentially exhibits the same behaviour observed for tests carried out under controlled fully-reversed strain (series 2A). However, it was possible to observe for very small strain amplitudes, in the elastic domain, that the material has a stabilized behaviour from the beginning of the cyclic loading. Furthermore, the hardening for larger strain amplitudes is not so pronounced and thus the transition between the hardening and softening behaviours is more gradual than that observed for tests carried out under controlled fully-reversed strain. Figure 5b presents the variation of the stress amplitude with the number of cycles for the welded material, resulted from tests carried out under controlled fully-reversed strain (series 2C). The comparison of this response with the corresponding response obtained for the base material allows the formulation of the following conclusions: i) for high strain range levels, the welded material do not exhibit a clear stabilized cyclic behaviour; ii) for low strain range levels it seems that the welded material presents a stabilized cyclic behaviour earlier than what expected for the base material, which can be explained by an higher yield stress or larger elastic domain of the welded material.

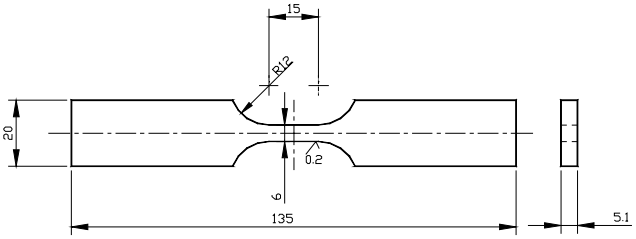

Figure 4. Specimen used in the characterization of the cyclic behaviour of the materials (dimensions in mm).

Table 4. Series of tests adopted for materials characterization.

Series Ref.	No. of Spec.	R_ε	Material	Series Ref.	No. of Spec.	R_σ	Material
2A	24	-1	Base material	**2E**	12	-1	Base material
2B	20	0	Base material	**2F**	12	0	Base material
2C	15	-1	Welded material	**2G**	12	-0.5	Base material
2D	11	0	Welded material	**2H**	10	-1	Welded material
				2I	11	0	Welded material

The BM exhibits, for tests performed under controlled tensile-mean-strain with null strain ratio (series 2B), a cyclic mean stress relaxation, which is illustrated in Fig. 6a. If the amount of plastic strain is appreciable, than a total cyclic mean stress relaxation is observed; if the amount of plastic strain is reduced or negligible the cyclic mean stress relaxation, if exists, is only partial. Ellyin (1997) observed similar behaviour for the ASTM A516 Gr. 70 steel. Figure 6b illustrates the variation of the cyclic mean stress for the WM tested under strain control with null strain ratio (series 2D). The WM shows a similar behaviour to the BM. The cyclic mean stress relaxes completely for higher strain ranges. For small strain ranges only a limited relaxation is observed. The minimum strain range above which the full mean stress relaxation occurs is higher for the WM.

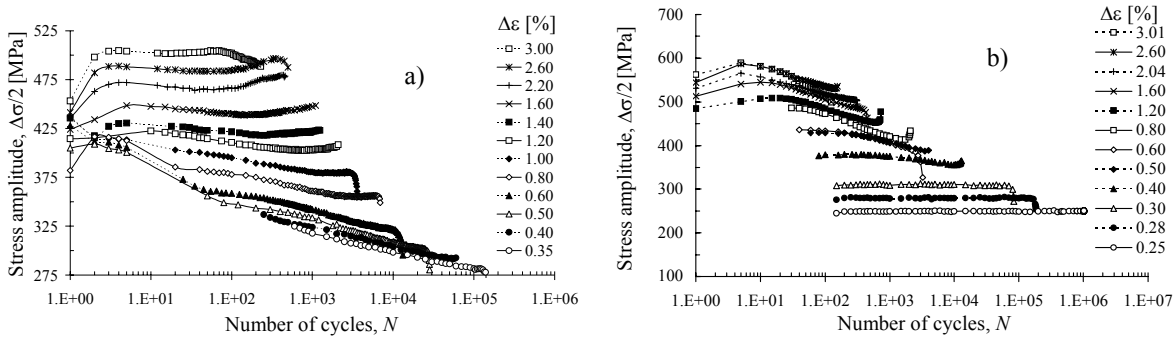

Figure 5. Evolution of the stress amplitude with the number of cycles and strain range: a) BM; b) WM.

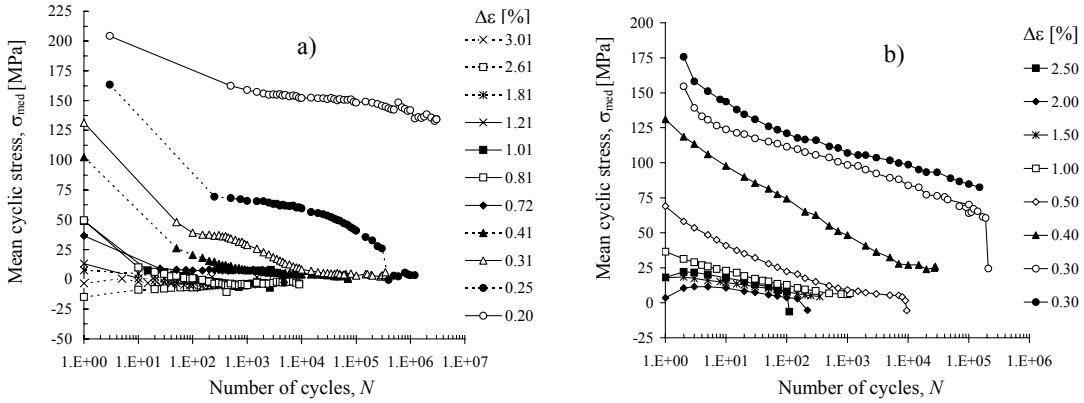

Figure 6. Evolution of the cyclic mean stress with the number of cycles and strain range: a) BM; b) WM.

The cyclic tests carried out under stress control conditions with non-null mean stress (series F and G) revealed, for the BM, the occurrence of cyclic creep strain or ratchetting strain, as mentioned by De Jesus *et al* (2005) and illustrated on Fig. 7. Figure 7 demonstrates that the amount of cyclic creep strain is a function of the stress amplitude and stress ratio. The BM exhibits higher cyclic creep strains for stress ratio R_σ=–0.5 than for stress ratio R_σ=0. Theoretically, for stress ratio R_σ=–1 the material should not present any cyclic creep strain. However, the cyclic tests of series 2E showed that for high stress amplitudes some cyclic creep strain for the BM which can be explained by some degree of anisotropy of the yield function, induced by the high plastic strain rate, or by some asymmetry on strain loading due to any eventual small deficiency on the placement of specimens on the test machine. The WM was tested under stress control only for two stress ratios, namely R_σ=0 and R_σ=–1 (series 2H and 2I). The analysis of the experimental data of the welded material stressed with R_σ=0 revealed that the material does not show any cyclic creep strain; an elastic shakedown is observed. For the stress ratio R_σ=–1 the WM exhibited some cyclic creep strain, but contrarily to the observed for the BM the cyclic creep strains can grow in positive or negative directions. The stress state for WM can be more complex than that expected for the BM since residual stresses and heterogeneities can be present on the WM.

5.2. Stabilized cyclic stress-strain relations

Both investigated BM and WM show stress-strain relations that vary with the applied load cycles due to several cyclic phenomena described in the previous section. Considering the stress-strain data from tests carried out under strain control, the most significant cyclic phenomena that affect its stabilization is the cyclic softening/hardening. A common practice is to consider a pseudo-stabilized behaviour which corresponds to the behaviour of the material at half life.

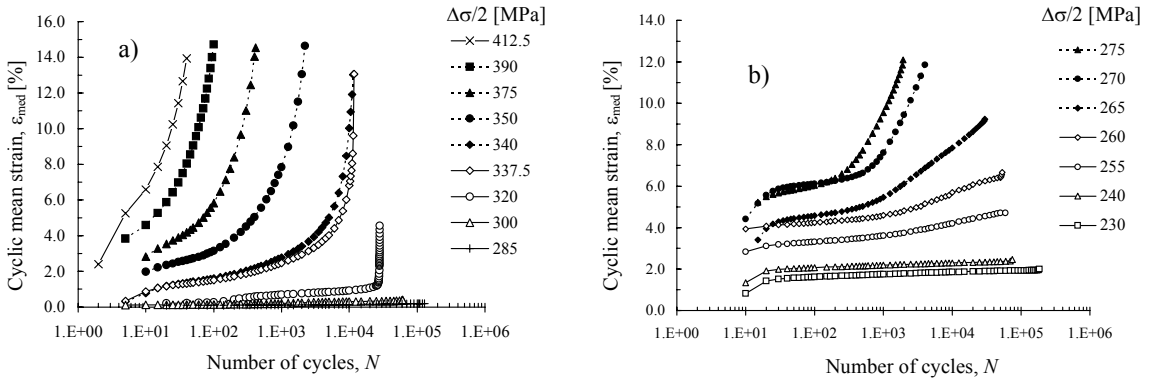

Figure 7. Cyclic creep strain or ratcheting strain obtained for the BM tested under stress control: a) R_σ=-0.5; b) R_σ=0.

Cyclic stress-strain curves were obtained for the BM and WM by plotting the stabilized half-life stress amplitude ($\Delta\sigma/2$) against the corresponding strain amplitude ($\Delta\varepsilon/2$). A cyclic stress-strain relation can be determined by adjusting, to the experimental data and using a best fit technique, the Ramberg-Osgood's relation (Ramberg and Osgood, 1943):

$$\frac{\Delta\varepsilon}{2} = \frac{\Delta\sigma}{2E} + \left(\frac{\Delta\sigma}{2K'}\right)^{1/n'} \tag{1}$$

where E is the young modulus, K' and n' are adjusting parameters, respectively the strain hardening coefficient and exponent. Figure 8 illustrates the experimental cyclic stress-strain data points and the fitted curves – the Ramberg-Osgood relations. The experimental points resulted from strain-controlled fatigue tests under fully-reversed tensile-mean-strain tests (series 2A, 2B, 2C and 2D). The curves were fitted to the fully-reversed and tensile-mean-strain data points together, since there are no significant differences between these two data sets. It can be concluded that the WM exhibits a cyclic yield stress larger than the BM. From the analysis of the curves it can be concluded that the two cyclic curves converge for a unique curve, for strain amplitudes larger than 2%. Table 5 summarizes the parameters K' and n' for the BM and WM. The BM and WM present a cyclic yield stress, defined for 0.1% of permanent strain, of 324 and 418 MPa, respectively. The strain ratio has no significant influence on stabilized strain-controlled test data.

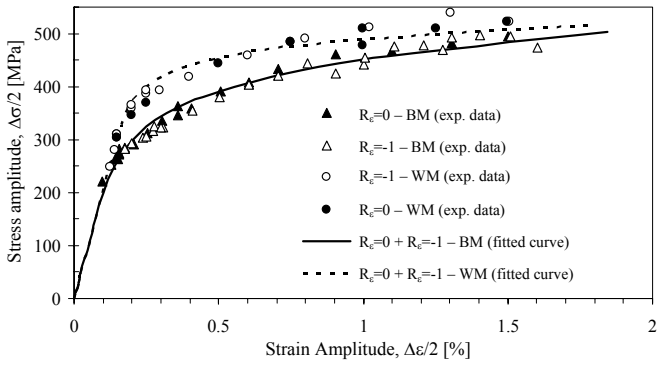

Figure 8. Cyclic curves of the base and welded materials.

Table 5. Cyclic properties of the base and welded materials.

Strain ratios	Base material				Strain ratios	Welded material			
	Cyclic curve		Master curve			Cyclic curve		Master curve	
	K′	n′	K^*	n^*		K′	n′	K^*	n^*
R_ε=-1	471.17	0.1682	400.00	0.1100	R_ε=-1	498.59	0.0744	510.00	0.1200
R_ε=0	466.62	0.1459	424.00	0.1200	R_ε=0	503.18	0.0834	-	-
R_ε=-1+ R_ε=0	468.13	0.1533	412.00	0.1150	R_ε=-1+ R_ε=0	499.84	0.0767	-	-

5.3. Description of the hysteresis loops

The superposition of stable fully-reversed hysteresis loops ($R_\varepsilon=-1$), with compressive tips placed at the origin of the coordinate system, showed that the ascending branches do not fall on a monotonically increasing unique curve for both BM and WM. Thus, both materials do not follow the Masing description: the positive branches of the hysteresis loops can not be described by the cyclic stress-strain curve, Eq. (1), magnified by a factor of two. Lefebvre and Ellyin (1984) and Ellyin (1997) suggested the description of the hysteresis loops for a non-Masing type material, through the application of the master curve concept. The master curve is obtained from matching the upper branches of the hysteresis loops through the displacement of each loop along its linear response portion as illustrated in Fig. 9. The equation of the master curve, in the referential with the origin coincident with the lowest tip of the hysteresis loop with the minimum proportional range, can be expressed as follows:

$$\Delta\varepsilon^* = \frac{\Delta\sigma^*}{E} + 2\left(\frac{\Delta\sigma^*}{2K^*}\right)^{1/n^*} \tag{2}$$

where K^* and n^* are constants; $\Delta\varepsilon^*$ and $\Delta\sigma^*$ are the strain and stress ranges evaluated in a coordinate system parallel to the original and with the origin coincident with the lowest tip of the hysteresis loop with minimum elastic domain. The relationship between the two coordinate systems, shown in Fig. 9, can be established using:

$$\begin{aligned} \Delta\sigma &= \Delta\sigma^* + \delta\sigma_0 \\ \Delta\varepsilon^p &= \Delta\varepsilon^{p*} \\ \Delta\varepsilon^e &= \Delta\varepsilon^{e*} + \frac{\delta\sigma_0}{E} \end{aligned} \tag{3}$$

where $\delta\sigma_0$ is the increase in the proportional stress limit – a measure of cyclic expansion of the elastic range. $\delta\sigma_0$ can be evaluated from Eqs. (1) to (3). Table 5 includes the values of the parameters K^* and n^* obtained using a best fitting technique.

From the analysis of Fig 9 it can be concluded that the BM has a deviation from Masing behaviour more pronounced than that observed for the WM. For the tested strain ranges the BM presents a higher expansion of its elastic range. Thus, the committed error when the cyclic curve is used to describe the hysteresis loops is lower for the WM.

Although tests conducted for WM under $R_\varepsilon=-1$ showed some deviations from Masing behaviour, tests carried for this steel under $R_\varepsilon=0$ showed practically a Masing behaviour. This is why Tab. 5 does not include the constants of the master curve for the WM under null-strain ratio.

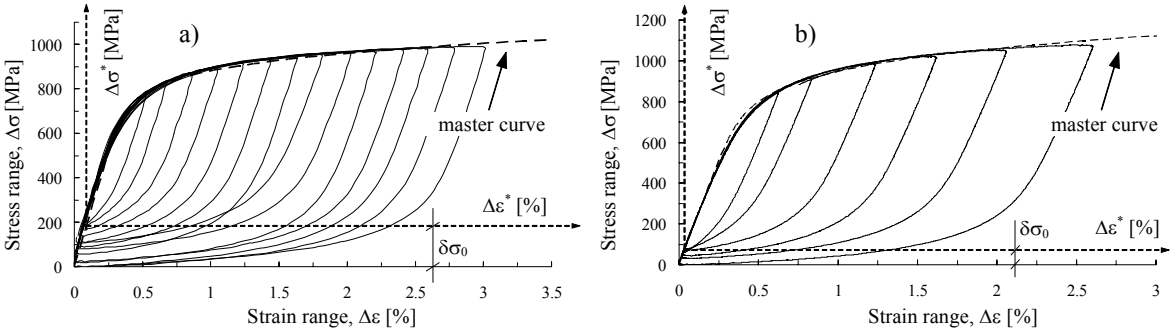

Figure 9. Master curves obtained with data for $R_\varepsilon=-1$: a) BM and b) WM.

6. Conclusions

A comparison between the cyclic elastoplastic behaviour of a BM – the P355NL1 steel – and a WM resulting from the automated submerged arc welding was characterized based on stress- and strain-controlled fatigue tests of smooth specimens. The comparison evidenced distinct behaviours between the welded and base materials, which justifies a more careful when the local approaches are applied in the analysis of welded details. The main conclusions of the comparison can be summarized as follows:

- Under strain-controlled cyclic tests the welded material do not exhibits a stabilization plateau for high plastic strain amplitude, as was observed in the base material. For small strain ranges, the welded material stabilizes earlier than the base material, which can be explained by a higher yield stress for the welded material.

- Under stress-controlled cyclic tests the welded material has more resistance to develop cyclic creep strains than base material. For example, for a cyclic load with null stress ratio, while the base material exhibits important cyclic creep strains the welded material suffers an elastic shakedown without any appreciable cyclic creep strain.

- The cyclic curve of the welded material shows a higher yield stress than the base material. However, the welded material has a lower strain hardening which leads to a convergence between the cyclic curves. The strain-ratio has a negligible effect on the stabilized cyclic stress-strain curve. The Ramberg-Osgood relation gives a good description of the cyclic curves.

- The BM and WM exhibit mean stress relaxation for tensile-mean-strain loading. The lowest strain range for which a complete mean stress relaxation still occurs is higher for the WM.

- Both materials present non-Masing behaviour, but the deviation from the Masing behaviour is more pronounced in the base material. For null strain ratios, the WM exhibits essentially Masing behaviour. The description of the hysteresis loops of the two materials can be well performed using the master curve concept.

The information provide in this paper is a valuable contribution for engineers concerned with the evaluation of fatigue damage parameters to be used in correlations with experimental fatigue data or in the assessment of fatigue actions for welded joints of pressure vessels or pressure vessel type details.

7. References

ASME – The American Society of Mechanical Engineers, 2001, "ASME Boiler and Pressure Vessel Code – Section VIII: Rules for Construction of Pressure Vessels, Division 2 – Alternative rules, Appendix 5: Design based on fatigue analysis", New York.

ASTM, American Society for Testing and Materials, 1998, "ASTM E606-92: Standard Practice for Strain-Controlled Fatigue Testing", In Annual Book of ASTM Standards, Part 10, pp. 557-571.

BSI – British Standards Institution, 2003, "PD 5500:2003, Specifications for unfired fusion welded pressure vessels", British Standard, London.

CEN, European Committee for Standardization, 2002, "EN 13445:2002 - Unfired Pressure Vessels", European Standard.

CEN, European Committee for Standardization, 2003, "EN 10028-3. Flat Products Made of Steels for Pressure Purposes - Part 3: Weldable Fine Grain Steels, Normalized", European Standard.

Chaboche, J.L., 1994, "Modelling of ratchetting: evaluation of various approaches", Eur. J. Mech., A/Solids, Vol.13, No. 4, pp. 501-518.

Cheng, G., Kuang, Z.B., Lou, Z.W., Li, H., 1996, "Experimental investigation of fatigue behaviour for welded joint with mechanical heterogeneity", International Journal of Pressure Vessel & Piping, Vol. 67, pp. 229-242.

Costa, J.D., Ferreira, J.M., 1993, "Fatigue crack initiation in notched specimens of 17Mn4 steel", Int. J. Fatigue, Vol.15, No. 6, pp. 501-507.

Cruz, J. A. M. P., Costa, J. D. M., Borrego, L.F.P., Ferreira, J.A.M., 2000, "Fatigue life prediction in AlMgSi1 lap joint weldment", International Journal of Fatigue, Vol. 22, pp. 601-610.

Curney, T. R., 1979, "Fatigue of welded structures", Cambridge University Press, 2nd Edition.

De Jesus, A.M.P., 2004, "Validação de Procedimentos de Cálculo à Fadiga de Reservatórios sob Pressão", PhD Thesis, University of Trás-os-Montes e Alto Douro, Vila Real, Portugal.

De Jesus, A.M.P, Ribeiro, A.S., Fernandes, A.A., 2005, "Low and High Cycle Fatigue and Cyclic Elasto-Plastic Behaviour of the P355NL1 Steel", Journal of Pressure Vessel Technology (submitted on December 2004, accepted for publication on June 2005).

DIN, Deutsche Institute for Standardization, 1983, "DIN 17102: Weldable Normalized Fine Grain Structural Steels. Technical Delivery Conditions for Plate, Strip, Wide Flats, Sections and Bars", Deutsche Norm.

Dowling, N.E., 1998, "Mechanical behaviour of materials: engineering methods for deformation, fracture and fatigue, 2nd ed., Prentice-Hall, New Jersey, USA.

EC, European Commission, 2001, "Pressure components fatigue design in the framework of directive 97/23/EC on pressure equipment. Final Report", DG-JRC/IAM, Petten – The Netherlands: http//www.ped.eurodyn.com/

Ellyin, F., 1997, "Fatigue Damage, Crack Growth and Life Prediction", Chapman & Hall, London, UK.

Higashida, Y., Burk, J.D., Lawrence, Jr., F.V., 1978, "Strain-controlled fatigue behaviour of ASTM A36 and A514 grade F steels and 5083-0 aluminium weld materials", Welding Journal, Vol.57, p. 334.

Jakubczak, H., Glinka, G., 1996, "Fatigue analysis of manufacturing defects in weldments", Int. J. Fatigue, Vol.8, No. 2, pp. 51-57.

Lawrence, F.V., Jr., Mattos, R.J., Higashida, Y., Burk, J.D., "Estimation the fatigue crack initiation life of welds", Fatigue Testing of weldments, ASTM STP 648, D. W. Hoeppner, Ed. American Society for Testing and Materials, pp. 134-158.

Lefebvre, D., and Ellyin, F., 1984, "Cyclic Response and Inelastic Strain Energy in Low Cycle Fatigue", International Journal of Fatigue, Vol. 6, No. 1, pp. 9-15.

Lemaitre, J., and Chaboche, J.L., 1990, "Mechanics of Solid Materials", Cambridge University Press, Cambridge, UK.

Radaj, D., and Sonsino, C. M., 1998, "Fatigue Assessment of Welded Joints by Local Approaches", Abington Publishing, Abington, UK.

Ramberg, W., and Osgood, W. R., 1943, "Description of Stress-Strain Curves by Three Parameters", Technical Report No. 902, National Advisory Committee for Aeronautics, NACA.

Ribeiro, A. S., 1993, "Efeito da fase de iniciação na previsão do comportamento à fadiga de juntas soldadas", PhD Thesis, University of Trás-os-Montes and Alto Douro, Vila Real, Portugal.

Ribeiro, A. S., De Jesus, A.M.P., Fernandes, A.A., 2001, "Fatigue life estimation of cruciform welded connections", COBEM 2001 – TBR1019, 16th Brazilian Congress of Mechanical Engineering, Uberlândia, MG, Brasil.

Taylor, N. et al, 2001, "Pressure Components Fatigue Design in the Framework of Directive 97/23/EC on Pressure Equipment", Final Report EC DG-ENTR, JRC-IAM.

Testin, R.A., Young, J.-L, Lawrence, Jr., F.V., Rice, R.C., 1987, "Predicting the fatigue resistance of steel weldement", Welding Journal, Vol. 66, No. 4, pp. 93-98.

Truchon, M., 1982, "Application of low-cycle fatigue test results to crack initiation from notches", Low-cycle fatigue and life prediction, ASTM STP 770, C. Amzallag, B.N. Leis, and P. Rabbe, Eds., American Society for Testing and Materials, pp. 254-268.

8. Responsibility notice

The authors are the only responsible for the printed material included in this paper.